Slip distribution of the M_w 5.9, 1999 Athens earthquake inverted from regional seismological data

David Baumont[1] and Francoise Courboulex
UMR Géosciences Azur, CNRS, Valbonne, France

Oona Scotti
IRSN/DPRE/SERGD/BERSSIN, Fontenay-aux-Roses, France

Nicos S. Melis and George Stavrakakis
NOA-IG, Athens, Greece

Received 25 October 2001; revised 11 February 2002; accepted 20 February 2002; published 3 August 2002.

[1] We studied the kinematic rupture process of the moderate magnitude (Mw 5.9), 1999 Athens earthquake using broadband seismic recordings at regional distances. The Apparent Source Time Functions (ASTF), obtained by retrieving the wave propagation and site effects from the seismic recordings using an empirical Green's function method, indicate a rather complex rupture with a source directivity primarily pointing towards Athens. To further characterize the faulting, we inverted the ASTFs for the kinematic history of the rupture using a damped-least square inversion scheme with inequality constraints. The rupture extent is delimited by a 10 km along-strike $\times$20 km along-dip zone. The mean slip amplitude on the observed rupture area is equal to 25 cm. The slip concentrates in two elongated zones with amplitudes reaching locally 60 cm. The total rupture lasted between 5 and 6 s. *INDEX TERMS:* 7215 Seismology: Earthquake parameters; 7255 Seismology: Surface waves and free oscillations; 7209 Seismology: Earthquake dynamics and mechanics

1. Introduction

[2] On September 7, 1999, a Mw 5.9 earthquake struck the city of Athens, causing the death of 143 people and injuring more than 2,000 others. Despite its moderate size, the material damages and the human loss were catastrophic, especially in the north-western suburbs of Athens where the macroseismic intensity reached IX [Figure 1]. This earthquake was the strongest event ever reported at such short distances (20 km) from the city.The scientific community has paid particular attention to this event, because it occured in a region where neither historical nor instrumental data have reported an event of such magnitude, and where none of the faults were recognized to be tectonically active [*Papadopoulos et al.*, 2000]. Although, two N120–130°, south dipping normal faults are clearly expressed on the morphology of the epicentral area (the Fili and Aspropyrgos faults), recent studies did not allow to determine which of these two faults was activated [for a review see *Papadopoulos et al.*, 2000; *Tselentis and Zahradnik*, 2000a and 2000b]. Source processes of moderate earthquakes are not well understood and yet they represent the main hazard for moderate seismicity regions such as Europe. Thanks to the newly upgraded broadband stations of the National Observatory of Athens (NOA) [Figure 1], the Athens earthquake and its largest aftershocks were recorded with a good azimuthal coverage and a sufficient signal to noise ratio, providing us with a good opportunity to better characterize the rupture process using regional seismic data. This study is part of the european project PRESAP (Practical, Real-time Estimation of Spatial Aftershock Probabilities) that aims to improve seismic hazard assessment in near-real time conditions.

2. Empirical Green's Functions

[3] Such a study of a moderate magnitude earthquake is based on the analysis of the seismic wave field at frequencies up to 0.1-to-few Hz. At these frequencies, the only realistic approach to remove both wave propagation and site effects from the seismograms, is the Empirical Green's Function (EGF) method. It consists in using as an empirical earth's impulse response, the record of a small earthquake having its hypocentral location and focal mechanism similar to that of the main event [*Hartzell*, 1978; *Mueller*, 1985; *Mori and Hartzell*, 1990; *Ammon et al.*, 1993; *Courboulex et al.*, 1998].

[4] To choose suitable EGFs among the early aftershocks of the Athens earthquake, we first selected the events located at distances smaller than 5 km from the mainshock hypocenter. Only events of magnitude larger than 3.8 were kept to ensure a good signal-to-noise ratio. As focal mechanisms can be mis-evaluated due to errors in the velocity model, we based our selection on the similarity of the waveforms produced by the mainshock and its aftershocks. This selection includes the 7 September 13:05:48 (M_L = 4.1), and 17:19:21 (M_L = 3.8), and 8 September 12:55:00 (M_L = 4.0) aftershocks. A *Posteriori* verification showed that the first two aftershocks and the mainshock have similar focal mechanism, whereas the third one differs from the others [*Papadopoulos et al.*, 2000; *Zahradnik*, 2002]. However, the use of this latter EGF led to results similar to those obtained using the first two EGFs.

[1]Now at IRSN/DPRE/SERGD/BERSSIN, Fontenay-aux-Roses, France.

0094-8276/02/2001GL014261$05.00

3. Apparent Source Time Functions

[5] Apparent Source Time Functions (ASTFs) were retrieved by deconvolving the EGFs from the mainshock recordings. This deconvolution was performed iteratively in the time domain using Ammon's approach [*personnal communication*] which includes a Gaussian filter (2 Hz) to get rid of the frequencies higher than the EGF corner frequency. Reliable ASTFs were obtained by using only the most energetic phases, i.e. the Rayleigh and Love waves, filtered (0.08 – 10 Hz) to insure a good signal-to-noise ratio.

[6] To check the quality of the results, we plotted in Figure 2 the recordings of the Rayleigh waves generated by the mainshock at the regional broadband network, and compared them to those predicted after iterative deconvolution. As one can notice, the fit is good for all the traces, except in this example at station NPS. For each wave type, the ASTFs and their uncertainties were determined by combining the results obtained using the three EGFs mentioned above.

[7] ASTFs were plotted in Figure 3 as a function of the azimuth of the stations. The shape and amplitude of the ASTFs vary smoothly with the azimuth, demonstrating the reliability of our determination. This reliability is also underlined by the similarity of the results derived for the Love and Rayleigh waves. The ASTFs are characterized by shorter durations at the stations located to the east (about 4s) than to the west (7s). This indicates a source directivity primarily pointing towards Athens, in good agreement with the distribution of damage [Figure 1], and preliminary studies [*Tselentis and Zahradnik*, 2000a]. However, a careful examination suggests that the rupture propagation is not unidirectional. As shown in Figure 3, the most impulsive ASTFs are observed at the stations PRK and NPS although they are located in very different azimuths. Moreover, the ASTFs obtained at the western stations are composed of at least three distinct pulses underlining the complex, heterogeneous character of the rupture.

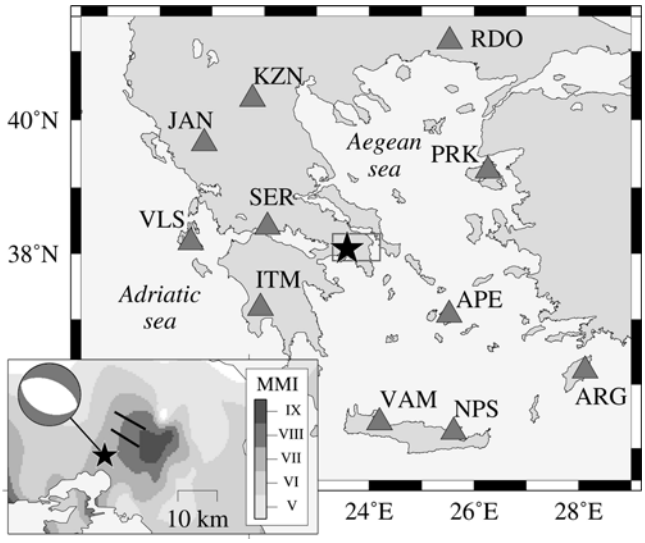

Figure 1. Location map of the NOA broadband stations used in this study (triangles) and the epicenter of the Athens 1999 earthquake (star). The station Sergoula (SER) is operated by the Patras and Prague Universities. The distribution of the Modified Mercalli Intensities relative to the Fili and Aspropyrgos faults (thick lines) are shown in the inset. The epicenter (star) and the normal fault focal mechanism were computed by *Papadopoulos et al.* [2000].

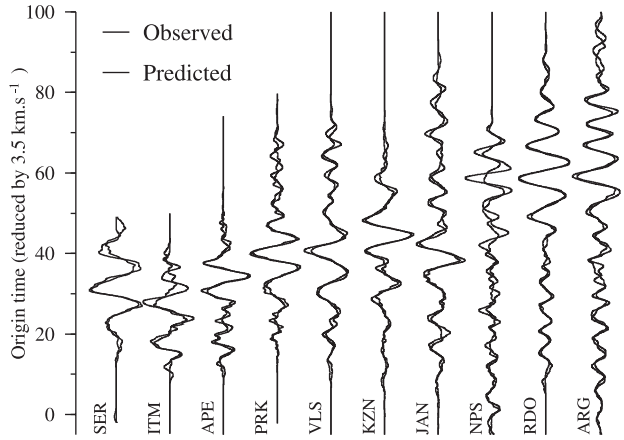

Figure 2. Comparison of the Rayleigh waves generated by the 1999 Athens earthquake and recorded at regional distances (thick lines), with the predicted ones after iterative deconvolution using the 7 September 13:05:48 EGF (thin lines). Traces are plotted with increasing distance from left to right.

4. Inversion for the Rupture History

[8] To further characterize the faulting, we inverted the ASTFs for the kinematic history of the rupture. The fault, assumed to be planar, was discretized into a regular grid. For each sub-fault k, we defined a slip amplitude, A_k, a rupture time, T_k, and a rise time, σ_k. To be consistent with the iterative deconvolution approach, the ASTFs were modeled as time series of normalized Gaussians:

$$ASTF(t) = \frac{4.\mu}{\sqrt{2.\pi}} \sum_k \frac{A_k}{\sigma_k} e^{-0.5\left(\frac{t-T_k-Tp_k}{\sigma_k}-2\right)^2} dxdy \qquad (1)$$

where Tp_k is the traveltime delay between the sub-fault k, and the nucleation point to the station, μ the rigidity, dx and dy the sub-fault dimensions. Tp_k was computed using the 8-s period phase velocities of the fundamental modes of Rayleigh and Love waves in the velocity model proposed by *Papadopoulos et al.* [2000] for the Attica region. The use of normalized Gaussians rather than boxcars (usually used in the parameterization of the forward problem), results only in minor changes in the slip distribution. Differenciating equation (1) leads to a non-linear matricial relation between data residuals and model parameters (i.e. A_k, T_k, σ_k). To optimize the inversion, we developed a damped least square iterative inversion scheme with inequality constraints [*Menke*, 1984]. These constraints were added to obtain physically realistic solutions: (1) $0 < A_k < 1.5m$, (2) $0.75\ V_s < r/T_k < 0.95\ V_s$, and (3) $0.5s < \sigma_k < 5s$. In order to obtain a smooth slip distribution, we defined a covariance matrix on the model parameters characterized by a correlation

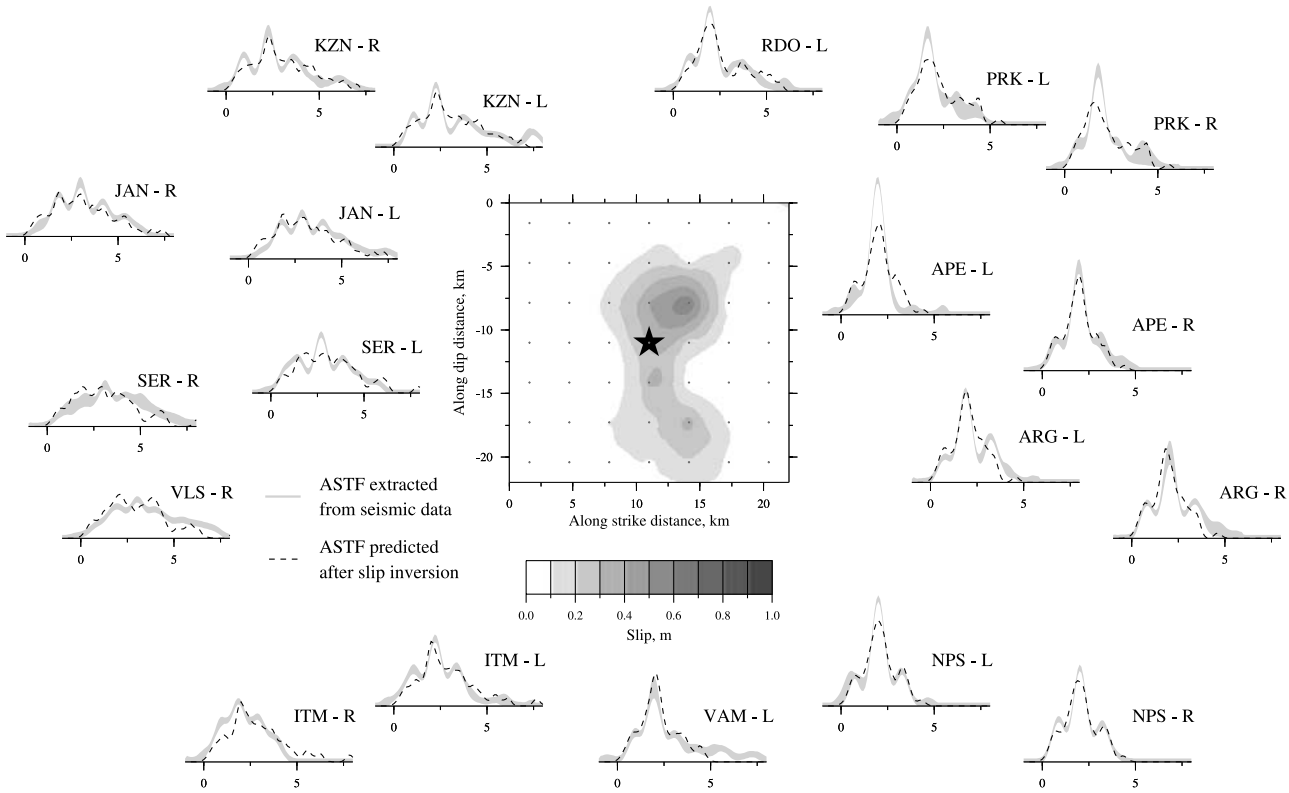

Figure 3. Azimuthal variations of the ASTFs obtained for the Athens earthquake on Rayleigh (R) and Love (G) waves (thick gray lines). The uncertainties are shown as shaded gray areas. The observed ASTFs were inverted for the kinematic rupture model of the event, including a smooth slip distribution shown in the center inset. The nucleation point (star) was centered on the fault. The ASTFs predicted by our rupture model (dashed black lines) are superimposed on the observations.

length, L. The uncertainties on data were introduced through a covariance matrix on data reduced to its diagonal elements. Nevertheless, as the least square criteria can be sensitive to a very small number of data with large errors, low weights were applied in the inversion to data with large deviations from the predicted values.

5. Athens Earthquake Slip Distribution

[9] Our fault model is composed of a single plane centered on the hypocenter. Its dimensions were fixed at 22×22 km^2 in order to include all the previous estimates of rupture area: 20×16 km^2 based on the aftershock distribution and forward modeling of the mainshock [*Tselentis and Zahradnik*, 2000b], and 10×11 km^2 by inverting SAR data [*Kontoes et al.*, 2000]. The fault strike and dip angles were fixed at 112° and 60° respectively as suggested by both the focal mechanism solution proposed by *Zahradnik* [2002] and the aftershock distribution [*Tselentis and Zahradnik*, 2000b]. Alternative fault geometries based on other studies were also tested such as a 39° dipping fault [*Papadopoulos et al.*, 2000; Harvard CMT catalog], however, the resulting rupture models are very similar to those obtained with the steeper fault. To model the asymmetry of the deformation field revealed by the SAR interferogram, *Kontoes et al.* [2000] considered a secondary fault, parallel to the main one and located at less than 5 km in the N-E direction. As this secondary fault is not required to explain the co-seismic rupture described by the ASTFs, it was not included in our fault model.

[10] The minimal resolution on the fault is given by the estimated area broken during the smallest aftershock, that is to say about 2×2 km^2. However, we chose a 3.0 km regular grid mesh, since the use of a denser grid did not significantly improve the data fit. The correlation length between the rupture model parameters was fixed by trial and error at 4 km. To test the reliability of the resulting kinematic rupture model, we performed the inversion using different starting models (homogeneous, central pulse, and checker board slip distributions), and found very similar results in terms of slip amplitudes, and overall shape of the rupture area.

[11] Figure 3 shows one of our best solutions as well as a comparison between the predicted and observed ASTFs. This rupture model satisfactorily predicts both the amplitudes and timing of the peaks observed in the ASTFs. Compared to the best homogeneous model ($L \times W = 7 \times 17$ km^2, rise time = 2 s, and slip = 30 cm), the data misfit was reduced by 70%. The main characteristics of the slip distribution are reasonably well constrained by the data as

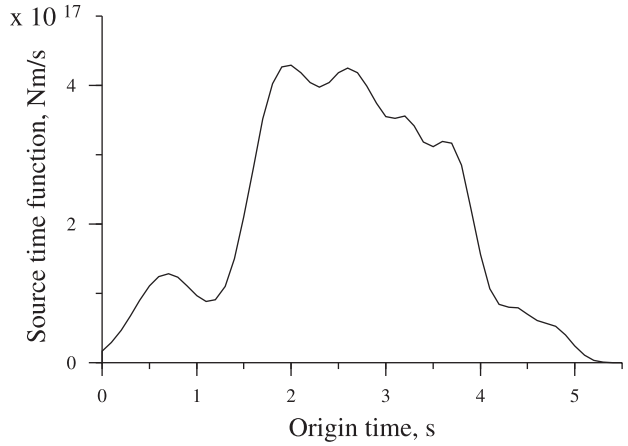

Figure 4. Source time function of the Athens earthquake obtained from the kinematic model solution using regional data with an EGF approach [Figure 3].

testified by high values of the diagonal elements of the resolution matrix. However, the rupture and rise time distributions are more poorly resolved and hence are not discussed here.

[12] As shown in Figure 3, the ruptured zone is mainly confined to a 10 km along-strike × 20 km along-dip area, a more elongated zone than the previous estimates mentioned above. The mean slip amplitude over the observed ruptured area is equal to 25 cm, close to the value we infered for the best homogeneous model and similar to the one obtained by *Kontoes et al.*, [2000]. It corresponds to a relatively low static stress drop (1 MPa). However, Figure 3 demonstrates that slip distribution is heterogeneous over the fault. The slip concentrates in two streched patches, located at about 5 km from the nucleation point, and reaching locally 60 cm in amplitude. An error on the slip distribution on the order of 10 to 20% was estimated by modeling the variation of the surface wave excitation with source depth. Such amplitude correction was not considered in our model due to large uncertainties on the hypocentral depth (13 ± 4 km).

[13] The rupture lasted about 5-to-6 s as revealed by the source time function derived from the inverted rupture model and plotted in Figure 4. This duration is in very good agreement with the estimation made by *Tselentis and Zahradnik* [2000b] by EGF forward modeling of the SER recordings whereas the rise time they suggested (0.1–0.3 s), may correspond to just the sharp but brief (0.5 s) increase we observed on the source time function, after a phase of weaker energy radiation.

6. Conclusions

[14] To better understand the rupture process of the 1999 Athens moderate earthquake, we analysed the broad-band seismograms recorded at regional distances by the NOA. The ASTFs determined using an empirical Green's function method, describe a rather complex rupture with a source directivity primarily pointing towards Athens. To further characterize the rupture, we inverted the ASTFs for its kinematic history using a damped-least square inversion scheme with inequality constraints.

[15] The rupture area was found to be mainly confined into a 10 km along-strike × 20 km along-dip zone with a mean slip amplitude equal to 25 cm which corresponds to a relatively low static stress drop of about 1 MPa. The slip concentrates in two elongated patches, both separated from the nucleation point by about 5 km, with amplitudes reaching locally 60 cm. The total rupture duration is of about 5-to-6 s.

[16] Further studies, also related to the project PRESAP, will aim to evaluate the ability of heterogeneous slip models to better predict the spatial aftershock distribution than homogeneous slip models.

[17] **Acknowledgments.** We thank the Prague Group for providing us the data at SERGOULA. We are also thankful to all the people who maintained the network. We are especially greatful to Chuck Ammon for his iterative deconvolution code. This work has been funded by the European project n° EVG1-CT-1999-00001 under contract IPSN-30000826. Publication Geosciences AZUR n° 425.

References

Ammon, C. J., A. A. Velasco, and T. Lay, Rapid estimation of rupture directivity: application to the 1992 Landers (Ms = 7.4) and Cape Mendocino (Ms = 7.2), California earthquakes, *Geophys. Res. Lett.*, *20*, 97–100, 1993.

Courboulex, F., M. A. Santoyo, J. F. Pacheco, and S. K. Singh, The 14 September 1995 (M = 7.3) Copala, Mexico, earthquake: A source study using teleseismic, regional, and local data, *Bull. Seis. Soc. Am.*, *87*, 999–1010, 1998.

Hartzell, S., Earthquake aftershocks as Green's functions, *Geophys. Res. Lett.*, *5*, 1–4, 1978.

Kontoes, C., P. Elias, O. Sykioti, P. Briole, D. Remy, M. Sachpazi, G. Veis, and I. Kotsis, Displacement field and fault model for the September 7, 1999 Athens earthquake inferred from ERS2 satellite radar interferometry, *Geophys. Res. Lett.*, *27*(24), 3989–3992, 2000.

Menke, W., Geophysical data analysis: Discrete inverse theory, Academic Press, Inc., 1984.

Mori, J., and S. Hartzell, Source inversion of the 1988 Upland, California, earthquake: Determination of a fault plane for a small earthquake, *Bull. Seis. Soc. Am.*, *80*, 507–518, 1990.

Mueller, C., Source pulse enhancement by deconvolution of an empirical Green's function, *Geophys. Res. Lett.*, *12*, 33–36, 1985.

Papadopoulos, G. A., G. Drakatos, D. Papanastassiou, I. Kalogeras, and G. Stavrakakis, Preliminary results about the catastrophic earthquake of 7 September 1999 in Athens, Greece, *Seis. Res. Lett.*, *71*(3), 318–329, 2000.

Tselentis, G.-A., and J. Zahradnik, Aftershock monitoring of the Athens earthquake of 7 September 1999, *Seis. Res. Lett., 71*, *7*(3), 330–337, 2000a.

Tselentis, G.-A., and J. Zahradnik, the Athens earthquake of 7 September 1999, *Bull. Seis. Soc. Am.*, *90*(5), 1143–1160, 2000b.

Zahradnik, J., Focal mechanism of the Athens 1999 earthquake by ASPO method, *submitted to Tectonophysics*, 2002.

D. Baumont and F. Courboulex, Géosciences Azur, 250 Av Einstein F-06560 Valbonne. (baumont@irsn.fr)

O. Scotti, IRSN/DPRE/SERGD/BERSSIN, 60-68 Av. du Général Leclerc, BP 6, F-92265 Fontenay-aux-Roses.

N. Melis and G. Stavrakakis, NOA-IG, P.O. Box 20048 Lofos Nymfon, GR-118 10, Athens, Greece.